Superstructural Description of Deformation Process in Uniaxial Extension of Preoriented Isotactic Polypropylene

KENJI YAMADA and MOTOWO TAKAYANAGI, *Department of Applied Chemistry, Faculty of Engineering, Kyushu University, Hakozaki, Fukuoka, 812, Japan*

Synopsis

The strains on uniaxial extension of preoriented isotactic polypropylene are separated over the whole range of deformation into three processes: crystallite boundary slip (A_1 process), uniform shear deformation of crystallites (A_2 process), and restoration of molecular orientation from the shear-deformed state ($\bar{A}_2$ process). They are separately evaluated by the use of the parameters of superstructure varying in deformation. Both the A_1 and A_2 processes predominate before the $A_2 \rightarrow \bar{A}_2$ transition takes place. Wide- and small-angle x-ray goniometries detect this transition. After the $A_2 \rightarrow \bar{A}_2$ transition takes place, the specimen cannot be deformed by the A_1 or A_2 process, but by a molecular process such as pulling out the isolated extending chains from the folded chain crystals followed by their refolding. From the quantitative evaluations of the strains associated with the A_1 and A_2 processes it is deduced that the initial shear compliance for the A_1 process is smaller than that for the A_2 process.

INTRODUCTION

Peterlin[1] reported in detail the superstructural change in the plastic deformation of bulk crystallized polymers. Analysis of the superstructural change in uniaxial extension for bulk crystallized polymers by means of x-ray goniometries appears more difficult, since they consist of lamellae that are statistically random oriented. On the other hand, preoriented crystalline polymers, in which the lamellae are almost regularly stacked, are more easily analyzed in detail with regard to the superstructural change in extension. Keller et al.[2,3] investigated the relationship between macroscopic deformation and superstructural change in uniaxial extension up to a strain of about 60% for preoriented low-density polyethylene which was drawn, rolled, and then annealed.

In this paper, a T-die sheet of isotactic polypropylene which possesses a relatively simple superstructure is uniaxially extended up to a strain of several hundred percent to elucidate various mechanisms of deformation causing superstructural changes in the whole range of deformation covering fiber formation. Such superstructural changes in a newly formed structure take place in large deformations up to several hundred percent. This strain is far larger than 60% which Keller et al.[2,3] have used. Wide-angle x-ray diffraction (WAXD) and the small-angle x-ray scattering (SAXS) are employed for detecting the changes of the superstructure. The superstructural change during uniaxial extension takes place with various deformation mechanisms. In this paper we tried to evaluate the strains of the specimen associated with various deformation mechanisms quantitatively as far as possible.

Journal of Applied Polymer Science, Vol. 24, 781–799 (1979)

0021-8995/79/0024-0781$01.00

EXPERIMENTAL

The specimen used is a T-die sheet of isotactic polypropylene (Noblen, MFI = 2.8) with a draw ratio of 5.2, which is wound up at 15 mm/min at 142°C after it is extruded from the T-die at 270°C. The specimen was cut from the T-die sheet in such a way that the angles between the testing direction and the molecular axis were 45° and 90°. The width, thickness, and gauge length of the specimen were 5, 0.3, and 20 mm, respectively. The specimen was uniaxially stretched at 40°, 100°, and 130°C at 5 mm/min with a tensile tester, Tensilon UTM-3 (Toyo Baldwin Co., Ltd.). The WAXD and SAXS images of unstretched and stretched specimens were taken with the x-ray generator Rotaunit (Rigaku Denki Co., Ltd.). Density was measured at 25°C by the floatation method using an ethanol–water system.

RESULTS AND DISCUSSION

Superstructure of T-Die Sheet of Isotactic Polypropylene

The superstructure of the specimen was examined by WAXD and SAXS by irradiating x-rays along the direction perpendicular to the surface of the T-die sheet (N direction), the one parallel to the machine direction (M direction), and the one parallel to the surface of the T-die sheet and perpendicular to the machine direction (T direction). Figure 1(a), 1(b), and 1(c) show the WAXD and SAXS photographs observed along the N, T, and M directions, respectively. In the WAXD and SAXS in the N and the T directions, the M direction accords with the meridional direction. Both the diffraction spots of (110) and (040) in the WAXD of the N direction and the T direction appear on the equator, and the ones in the M direction are almost distributed in Debye rings. In the SAXS of the N and the T directions, the diffraction spots appear on the meridian, and diffuse diffraction is found along the equator. In the SAXS of the M direction, the diffuse diffraction only is found along the equator. These WAXD and SAXS observations show that lamellar crystals composed of crystallites are stacked along the M direction and the molecular axis is oriented parallel to it. The crystallites are also the structure elements of the microfibrils which orient parallel to the M direction. Therefore, the superstructure of the T-die sheet of isotactic polypropylene viewed along the N direction may be as schematically shown in Figure 2. As tie molecules might be formed in the fiber structure according to Takayanagi et al.[4–6] and Peterlin,[7] they are shown by solid lines in the amorphous region in Figure 2. The tie molecules cannot be detected by means of x-ray diffraction, but sustain the major part of the load acting on the specimen during deformation.

Observation of Superstructural Change in Uniaxial Extension

When the specimen is uniaxially extended at angle θ of 45° or 90° which forms between the testing direction and the molecular axis, the width of the specimen decreases much more than the thickness.[9] In this case, only the width reduction of the specimen is taken into account, and therefore the macroscopic deformation of the specimen is simplified to a two-dimensional deformation. Figure 3(a) shows the WAXD and SAXS photographs taken with the x-ray beam irradiating

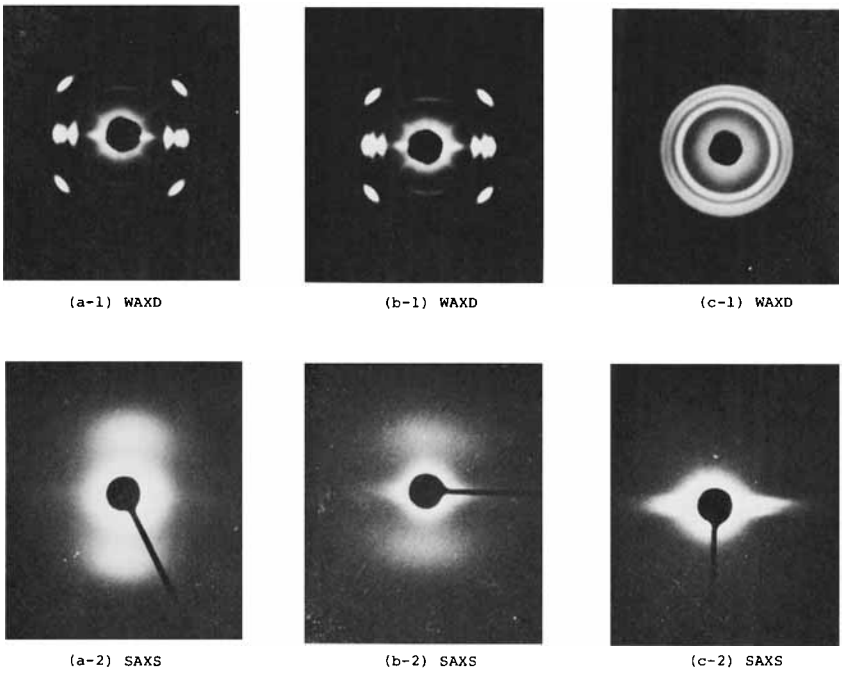

Fig. 1. (a) WAXD(a-1) and SAXS(a-2) photographs for the T-die sheet of isotactic polypropylene; x-ray beam is irradiated along normal (N) direction; machine (M) direction accords with the meridional direction. (b) WAXD(b-1) and SAXS(b-2) photographs for the same sample as in (a); x-ray beam is irradiated along transverse (T) direction; M direction accords with the meridional direction. (c) WAXD(c-1) and SAXS(c-2) photographs for the same sample as in (a); x-ray beam is irradiated along M direction. T direction accords with the meridional direction.

along the N direction for the sample of $\theta = 45°$ drawn to the draw ratio λ of 1.3 at 100°C. The meridional direction is coincident with the testing direction. The azimuthal angle of the (040), or (110), diffraction spot forming to the equator is denoted by ϕ, the azimuthal angle of the diffraction spot of SAXS forming against the meridian is denoted by ω, and the angle of the direction of the diffused scattering of SAXS against the equator is denoted by η, Figure 3(b). Figure 3(c) shows the relationship between the observed angles of the ϕ, ω, and η and the corresponding superstructure; ϕ is the angle between the chain direction and the testing direction, ω is the angle between the lamellar normal plane and the testing direction, and η is the angle between the microfibril direction and the testing direction.

When the specimen with the superstructure schematically shown in Figure 2 is uniaxially extended in such a way that the angle between the testing direction and the molecular axis is θ, it may be conceivable that the superstructural change takes place by three types of deformation mechanism shown in Figure 4.[8,9] Figure 4(a) shows the B process associated with the slip in the interlamellar amorphous region, in which neither ϕ nor ω change during extension, but η decreases. Figure 4(b) shows the A_1 process associated with the intercrystallite boundary slip, in which ϕ, ω, and η decrease in the same manner during extension. Figure 4(c) shows the A_2 process associated with the uniform shear deformation of crystallites, in which angle $(\omega - \phi)$ increases monotonously during extension.

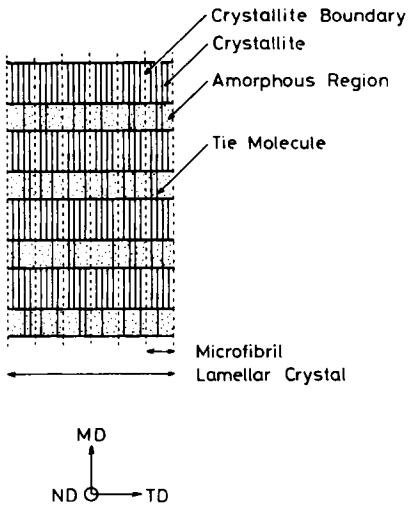

Fig. 2. Schematic representation of superstructure of the T-die sheet of isotactic polypropylene viewed along the N direction.

Effects of Testing Direction on Various Deformation Mechanisms

Figures 5(a), 5(b), and 5(c) show the variation of ϕ, ω, and $(\omega - \phi)$ as a function of the natural logarithm of the ratio of width reduction, ϵ_W, in uniaxial extension for $\theta = 45°$ and 90° at 100°C, respectively. The ϵ_W is evaluated by the following equation:

$$\epsilon_W = \ln \frac{W_0}{W}$$

where W_0 and W are the widths of the specimen before and after stretching, respectively. The width reduction of the specimen is much larger than the thickness reduction,[9] and therefore the value of ϵ_W is assumed to be nearly equal to the true strain of the specimen. The strain associated with the width reduction,

$$e_W = \frac{W_0}{W} - 1$$

may be nearly equal to the strain of the specimen if the volume of the specimen does not change with extension. Figure 6(b) shows the variation of ϕ and η as a function of ϵ_W in extension for $\theta = 45°$ at 100°C. Since the η curve is approximately coincident with the ϕ curve, the B process need not be taken into account. According to Figure 5, the ϕ curve monotonously decreases with increasing ϵ_W, whereas the ω curve increases up to $\epsilon_W \simeq 0.66$ ($e_W \simeq 0.93$) and then decreases. Thus, the $(\omega - \phi)$ curve takes a maximum at $\epsilon_W \simeq 0.66$ ($e_W \simeq 0.93$) for $\theta = 45°$. This shows that the A_2 process takes place. In the region of $\epsilon_W \geq 0.66$ ($e_W \geq 0.93$), the $(\omega - \phi)$ curve decreases and a restoration of molecular orientation takes place from the shear-deformed state, as shown in Figure 7. This deformation mechanism is termed the $\bar{A}_2$ process.

In uniaxial extension for $\theta = 90°$ at 100°C, both the ϕ and ω curves decrease, but the $(\omega - \phi)$ curve does not change in the region of $\epsilon_W \leq 0.3$ ($e_W \leq 0.3$), as shown in Figure 5. This fact is explained by the A_1 process that takes place

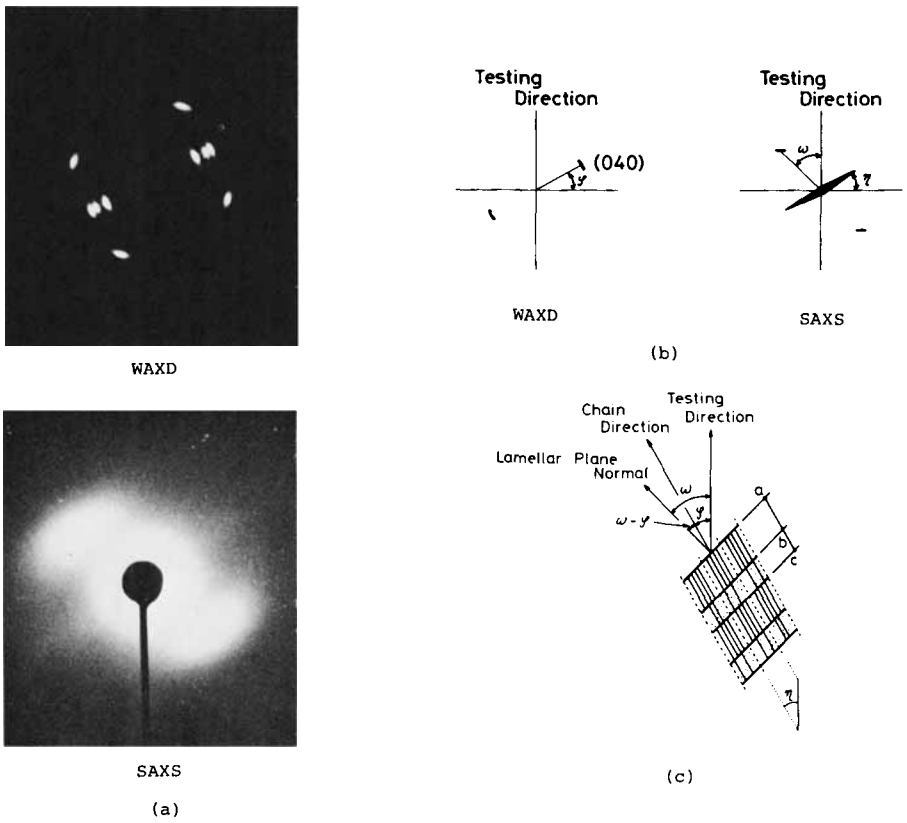

Fig. 3. (a) WAXD and SAXS photographs taken with the x-ray beam irradiating along the N direction for the sample of $\theta = 45°$ drawn to the draw ratio of 1.3 at 100°C. (b) Schematic representation of main spots in WAXD and SAXS photographs shown in Fig. 3(a); ϕ is the azimuthal angle of the (040), or (110), diffraction spot measured from equator, and ω and η are the azimuthal angles of the scattering spot of SAXS measured from the meridian and the diffused scattering of SAXS measured from the equator, respectively. (c) Relationship between the ϕ, ω, and η angles measured in Fig. 3(b) and the corresponding superstructure.

preferentially due to the larger normal stress exerting on intercrystallite boundary which is effective in separating the crystallites in lamellar crystals. In the region of $0.3 \leq \epsilon_W \leq 1.1$ ($0.3 \leq e_W \leq 2.0$), the $(\omega - \phi)$ curve increases with increasing ϵ_W, indicating that the A_2 process takes place, whereas for $\epsilon_W \geq 1.1$ ($e_W \geq 2.0$), the $(\omega - \phi)$ curve decreases with increasing ϵ_W, indicating that the $\bar{A}_2$ process takes place.

Effects of Testing Temperature on Various Deformation Mechanisms

Figures 6(a) and 6(c) show that the η curve is almost coincident with the ϕ curve in extension for $\theta = 45°$ at 40°C and 130°C as well as 100°C mentioned above. This means that the B process need not be taken into account at any temperature. Tie molecules are rigid enough to keep the shape of the amorphous region like the crystalline region, even though some loose molecules undergo thermal motion in the amorphous region. Figures 8(a), 8(b), and 8(c) show the variation of ϕ, ω, and $(\omega - \phi)$ as a function of ϵ_W in extension for $\theta = 45°$ at 40°C,

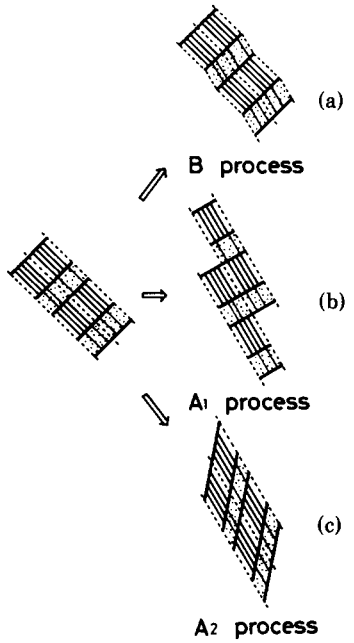

Fig. 4. Schematic representation of the deformation of the B, A_1, and A_2 processes in uniaxial extension of the oriented specimen such as the T-die sheet of isotactic polypropylene: (a) B process; (b) A_1 process; (c) A_2 process.

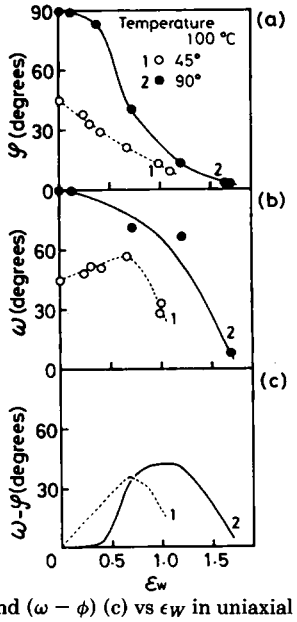

Fig. 5. Values of ϕ (a), ω (b), and $(\omega - \phi)$ (c) vs ϵ_W in uniaxial extension for $\theta = 45°$ and 90° at 100°C.

100°C, and 130°C, respectively. It is noted that the ϕ curve is not affected by the testing temperature, but both the ω and $(\omega - \phi)$ curves are somewhat dependent on the testing temperature. The maximum of the $(\omega - \phi)$ curve is found at lower ϵ_W with increasing testing temperature.

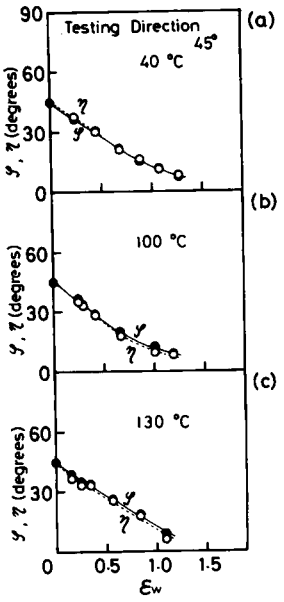

Fig. 6. Values of ϕ and η vs ϵ_W in uniaxial extension for $\theta = 45°$ at 40°C (a), for $\theta = 45°$ at 100°C (b), and for $\theta = 45°$ at 130°C (c).

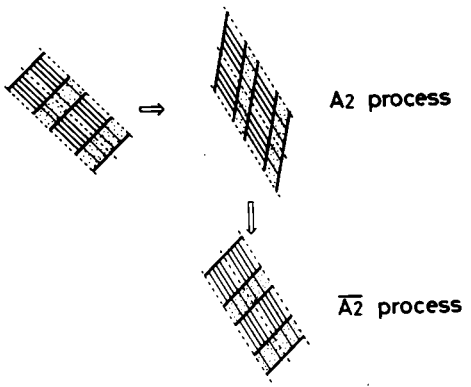

Fig. 7. Schematic representation of the $\overline{A}_2$ process in uniaxial extension of the oriented specimen such as the T-die sheet of isotactic polypropylene.

Change in Long Period During Uniaxial Extension

If the sum ($\overline{ac}$) of the original thickness of crystallites, $\overline{ab}$, and the original thickness of the interlamellar amorphous region, $\overline{bc}$, does not vary during extension, as shown in Figure 3(c), the long period L_C at the intermediate stage of extension is calculated by the use of ($\omega - \phi$) as follows:

$$L_C = (\overline{ab} + \overline{bc}) \cos (\omega - \phi)$$

Figures 9(a) and 9(b) show the relationship between the long period and the ϵ_W in extension for $\theta = 45°$ and 90° at 100°C and for $\theta = 45°$ at 40°C, 100°C, and 130°C, respectively. As shown in Figure 9(a), the observed curves (solid lines) are approximately coincident with the calculated curves (dotted lines) in extension for both $\theta = 45°$ and 90° at 100°C. As shown in Figure 9(b), the observed

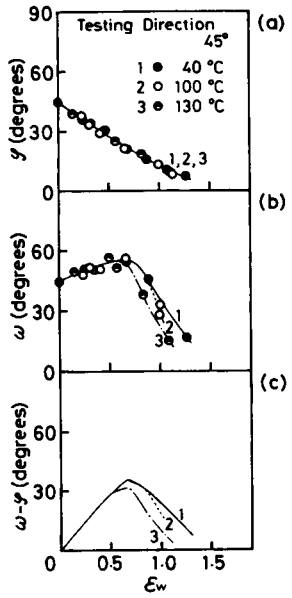

Fig. 8. Values of ϕ (a), ω (b), and $(\omega - \phi)$ (c) vs ϵ_W in uniaxial extension for $\theta = 45°$ at 40°C, 100°C, and 130°C.

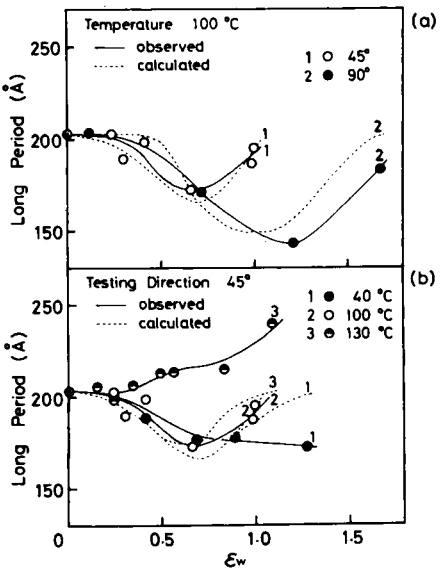

Fig. 9. Long period vs ϵ_W in uniaxial extension for $\theta = 45°$ and 90° at 100°C (a) and for $\theta = 45°$ at 40°C, 100°C, and 130°C (b).

curves deviate from the calculated curves above $\epsilon_W \simeq 0.75$ ($e_W \simeq 1.1$) in extension for $\theta = 45°$ at 40°C, and above $\epsilon_W \simeq 0.3$ ($e_W \simeq 0.3$) in extension for $\theta = 45°$ at 130°C. The thickness of the crystallites, l_C, is evaluated by the following equation:

$$l_C = LV_C \tag{1}$$

where the L is the observed long period and V_C is the volume fraction crystallinity

evaluated by the use of the specimen density. In this case the densities of the crystalline region and the amorphous region are assumed to be 0.9349 and 0.8565 g/cm^3, respectively.[10] In all testing conditions, the curves of the thickness of the crystallites evaluated by eq. (1) also begin to deviate from the curves calculated by the formula of $L_C V_C$ in the regions of the $A_2 \rightarrow \overline{A}_2$ transition.[9] It also becomes apparent that the thickness of the crystallites depends on the testing temperature after the $A_2 \rightarrow \overline{A}_2$ transition takes place.[9]

Quantitative Evaluation of Strains Associated with Various Deformation Mechanisms

The method of Young et al.[11] is extended for quantitative evaluation of the strains of the A_1, A_2, and $\overline{A}_2$ processes.

Method of Quantitative Evaluation

Deformation Process in the Earlier Stage of Extension. Figure 10 shows the relationship between the macroscopic deformation of the preoriented specimen and the superstructural change in (a) the A_1 process and (b) the A_2 process. The TE_0 and TE in the figure denote the testing directions before and after extension, respectively, and C is the direction of the molecular axis. The figure is drawn in such a way that the chain directions before and after extension are made to coincide. In actual testing conditions, the directions of TE_0 and TE always are the same. The portions on and below the C line in the figure show the specimens before and after extension, respectively. The ϕ_0, ω_0, and W_0 are the angle between the molecular axis and the testing direction, the angle between the lamellar normal plane and the testing direction, and the width of the sample,

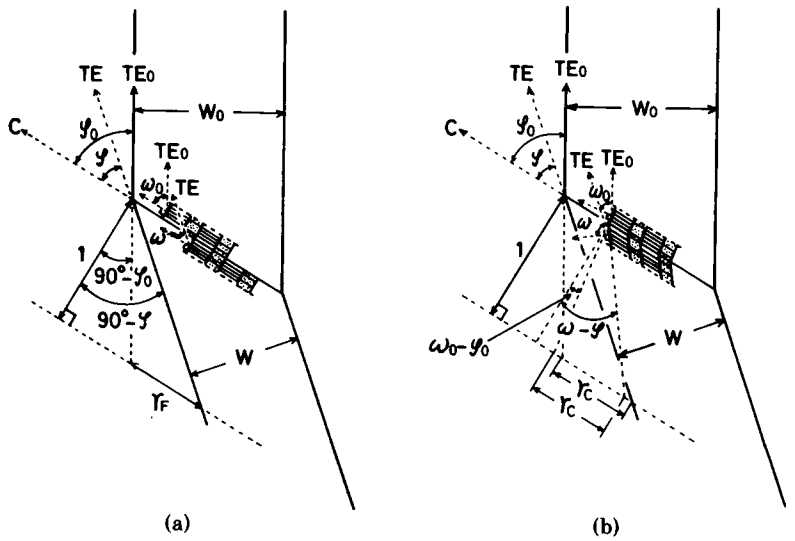

Fig. 10. Relationship between the macroscopic deformation of the specimen and the superstructural change in (a) the A_1 process and (b) the A_2 process. TE_0 and TE denote the testing directions before and after uniaxial extension, respectively, and C, the direction of molecular axis.

respectively, before extension. The ϕ_0, ω_0, and W_0 change into ϕ, ω, and W, respectively, after extension. As shown in Figure 10(a), if one draws a line which is parallel to the C line and is a unit length apart from the C line, it can be shown that the shearing strain for the A_1 process, γ_F, is

$$\gamma_F = \cot \phi - \cot \phi_0 \tag{2}$$

Since the value of $(\omega - \phi)$ does not change during extension in the A_1 process,

$$\omega_0 - \phi_0 = \omega - \phi = \text{const} \tag{3}$$

If $W_{\gamma F}$ is the width of the sample, W, after extension in the case of the A_1 process, we obtain

$$W_{\gamma F}/W_0 = \sin \phi/\sin \phi_0 \tag{4}$$

If both sides of eqs. (2), (3), and (4) are differentiated by ϕ, respectively, we obtain

$$d\phi = -d\gamma_F \sin^2 \phi \tag{5}$$

$$d\omega = d\phi = -d\gamma_F \sin^2 \phi \tag{6}$$

$$dW_{\gamma F}/W_{\gamma F} = \cot \phi \, d\phi \tag{7'}$$

The substitution of eq. (5) in eq. (7') results in

$$-dW_{\gamma F}/W_{\gamma F} = d\gamma_F \sin \phi \cos \phi \tag{7}$$

As shown in Figure 10(b), the shearing strain for the A_2 process is

$$\gamma_C = \cot \phi - \cot \phi_0 \tag{8}$$

similar to the A_1 process. The strain γ_C is also evaluated on the basis of the change in $(\omega - \phi)$:

$$\gamma_C = \tan(\omega - \phi) - \tan(\omega_0 - \phi_0) \tag{9}$$

When $W_{\gamma C}$ is the width of the specimen, W, after extension in the A_2 process,

$$W_{\gamma C}/W_0 = \sin \phi/\sin \phi_0 \tag{10}$$

From eq. (8) we obtain

$$d\phi = -d\gamma_C \sin^2 \phi \tag{11}$$

The substitution of eq. (11) in eq. (9), after both sides of eq. (9) have been differentiated by ϕ, results in

$$d\omega = d\gamma_C \, [\cos^2(\omega - \phi) - \sin^2 \phi] \tag{12}$$

Similarly,

$$-dW_{\gamma C}/W_{\gamma C} = d\gamma_C \sin \phi \cos \phi \tag{13}$$

Figure 11 is a schematic representation of the superstructural changes in the A_1 process represented by eqs. (2), (3), and (4), (a) → (b), and in the A_2 process represented by eqs. (8), (9), and (10), (a) → (c). The black spots in the figure show the mass centers of the crystallites. When the value of ϕ decreases to 0°, the values of γ_F and γ_C both infinitely increase and the value of W decreases to 0, according to eqs. (2), (3), (4), (8), (9), and (10). Therefore, the black spots

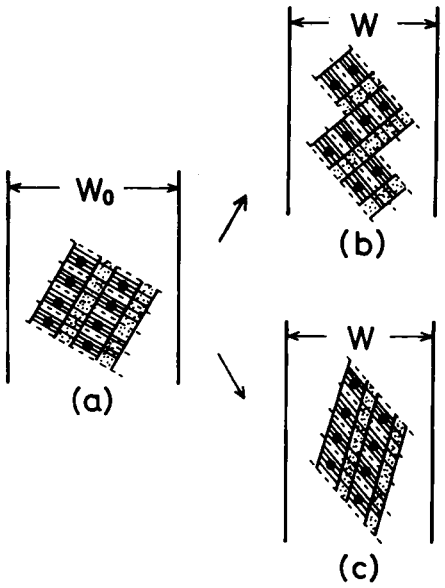

Fig. 11. Schematic representation of the superstructural changes in the A_1 process represented by eqs. (2), (3), and (4), (a) → (b), and in the A_2 process represented by eqs. (8), (9), and (10), (a) → (c).

in the figure gather toward the center line of the width of the specimen during uniaxial extension.

When both the A_1 and A_2 processes take place before the $A_2 \rightarrow \overline{A}_2$ transition (Fig. 7), the minute change $d\phi$ in the angle ϕ consists both of the contribution from the A_1 process, $d\phi(F)$, and the one from the A_2 process, $d\phi(C)$; and the minute change $d\omega$ in the angle of ω also consists of both $d\omega(F)$ and $d\omega(C)$. By solving the simultaneous equations $d\phi = d\phi(F) + d\phi(C)$ and $d\omega = d\omega(F) + d\omega(C)$, we obtain

$$d\gamma_F = -[\{\cos^2(\omega - \phi) - \sin^2\phi\}\, d\phi + \sin^2\phi\, d\omega]/\sin^2\phi \cos^2(\omega - \phi) \quad (14)$$

$$d\gamma_C = (d\omega - d\phi)/\cos^2(\omega - \phi) \quad (15)$$

Therefore, the total of the minute amounts $d\gamma_F$ and $d\gamma_C$, γ_F and γ_C, respectively, are given by eqs. (16) and (17), respectively:

$$\gamma_F = -\int_{\phi_0}^{\phi} [\{\cos^2(\omega - \phi) - \sin^2\phi\}/\sin^2\phi \cos^2(\omega - \phi)]d\phi - \int_{\omega_0}^{\omega} \{1/\cos(\omega - \phi)\}\, d\omega \quad (16)$$

$$\gamma_C = -\int_{\phi_0}^{\phi} [1/\cos^2(\omega - \phi)]\, d\phi + \int_{\omega_0}^{\omega} [1/\cos^2(\omega - \phi)]\, d\omega \quad (17)$$

Similarly, the total amount of the minute decrease in width of the specimen, $(W_0 - W)$, at $\gamma_F = \gamma_F$ and $\gamma_C = \gamma_C$ is given by eq. (18) by using eqs. (7) and (13):

$$W_0 - W = \int_0^{\gamma_F} W \sin\phi \cos\phi\, d\gamma_F + \int_0^{\gamma_C} W \sin\phi \cos\phi\, d\gamma_C \quad (18)$$

where $W_{\gamma_F} = W_{\gamma_C} = W$.

Deformation Process in the Latter Stage of Extension. The deformation of specimen proceeds with the $\bar{A}_2$ process in the latter stage of extension. The $\bar{A}_2$ process, which gives rise to the decrease in the $(\omega - \phi)$ value, is caused not only by restoration of the shear-deformed crystallites to the orientation as found in the undeformed state, but also by the formation of new crystallites due to refolding of the chains once unfolded by stretching of the tie molecules.[8,9,12] The molecular axis in these newly born crystallities is almost perpendicular to the end plane of the crystallities. After the $A_2 \rightarrow \bar{A}_2$ transition takes place, the strain of the specimen might be calculated on the assumption that the A_2 process is caused by the restortion of the orientation in shear-deformed crystallites to the orientation in the original state without the formation of new crystallites (case 1) or the formation of new crystallites (case 2). Therefore, eqs. (16), (17), and (18) can be applied to case 1 in the latter stage of extension. On the other hand, case 2 cannot be described only by the x-ray goniometries when the A_1 process simultaneously takes place. Therefore, if the value of ϕ is decreased only by the A_1 process (case 2-1), we obtain

$$\gamma_F = -\int_{\phi_i}^{\phi} (1/\sin^2 \phi)\, d\phi \tag{19}$$

$$\gamma_C = 0 \tag{20}$$

$$W_0 - W = \int_{\gamma_{Fi}}^{\gamma_F} W \sin \phi \cos \phi \, d\gamma_F \tag{21}$$

where ϕ_i and γ_{Fi} are the values of ϕ and γ_F in the region of the $A_2 \rightarrow \bar{A}_2$ transition, respectively.

On the other hand, if, in case 2, only the microfibrils are deformed without giving rise to the A_1 process (case 2-2), we have

$$\gamma_F = 0 \tag{22}$$

$$\gamma_C = 0 \tag{23}$$

$$W_0 - W = W_i - W_{\text{obs}} \tag{24}$$

where W_i and W_{obs} are the widths of the specimen just before the $\bar{A}_2$ process starts and after it starts, respectively.

Method of Calculation

The differences between the boundary values of each small section, which is obtained by dividing the ϕ and ω curves shown in Figure 5 by the width of $e_W = 0.1$, are used as the values of $d\phi$ and $d\omega$, respectively, in eqs. (16), (17), and (19). The values in the center of each small section of the ϕ and ω curves are used as the ϕ and ω values in calculating eqs. (16), (17), (18), (19), and (21), respectively. From $d\phi$, $d\omega$, ϕ, ω, and eqs. (16) through (24), the value of the shearing strain on the intercrystallite boundary, γ_F, the value of the shearing strain on the intermolecular axis of crystallites, γ_C, and the amount of decrease in the width of the specimen, $(W_0 - W)$, are calculated.

Strains of Specimen Associated with Various Deformation Mechanisms

Figure 12 shows the relationships between the strains of the specimen calculated for case 1, case 2-1, and case 2-2. The data were taken from the uniaxial extension of the T-die sheet of isotactic polypropylene (a) for $\theta = 45°$ at 40°C, (b) for $\theta = 45°$ at 100°C, (c) for $\theta = 45°$ at 130°C, and (d) for $\theta = 90°$ at 100°C. For $\theta = 45°$, except in Figure 12(d), the strain curves calculated by eq. (18) (dotted lines) are in fairly good agreement with the observed ones (solid lines) insofar as the stain is smaller than that indicated by the arrows in the figure. The arrows

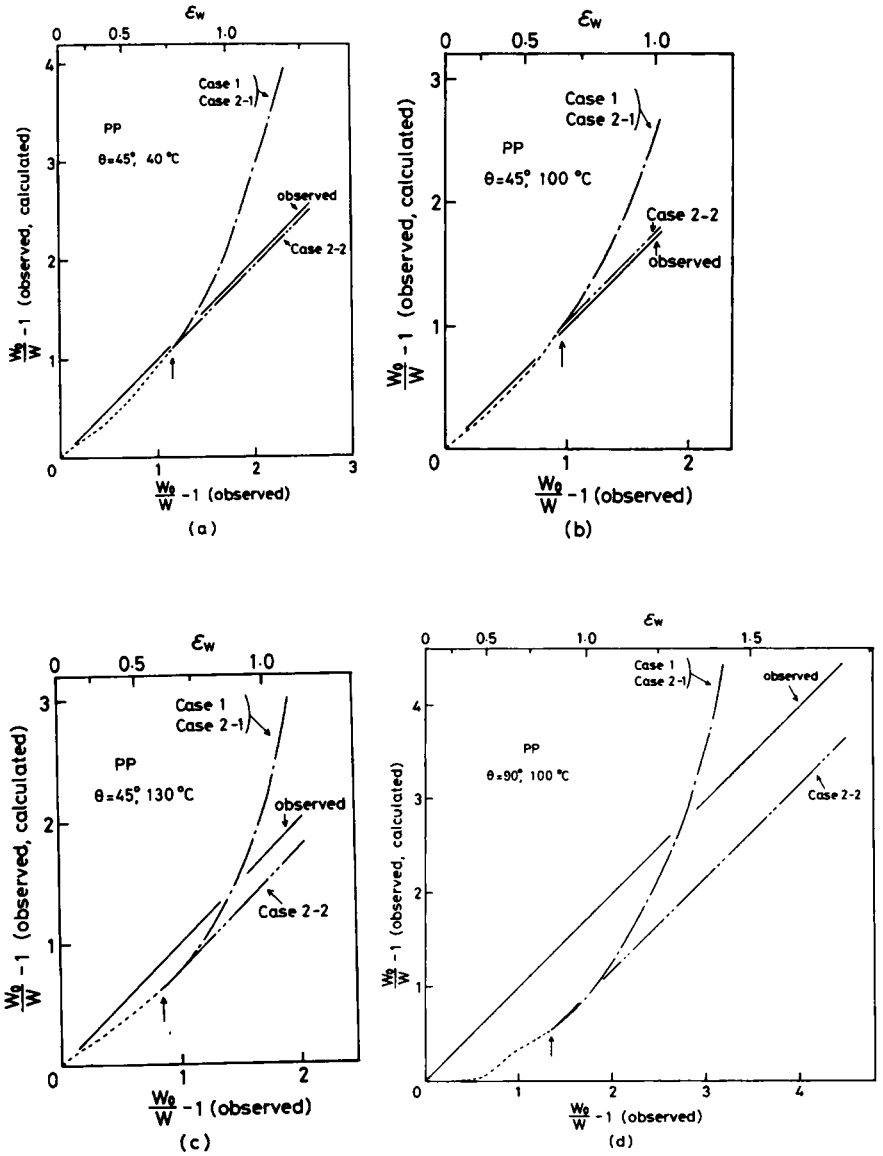

Fig. 12. Relationships between strains of the specimen calculated for case 1, case 2-1, and case 2-2. Data were taken from uniaxial extension for $\theta = 45°$ at 40°C (a), for $\theta = 45°$ at 100°C (b), for $\theta = 45°$ at 130°C (c), and for $\theta = 90°$ at 100°C (d). Arrows in the figure show the calculated strains of the specimen at the region of initiating the $\overline{A}_2$ process.

indicate the regions of initiating the $\overline{A}_2$ process. In the extension after these regions, the strain curves of case 1 and case 2-1, which are calculated by eqs. (18) and (21), respectively, are shown by the one dot–dash lines in the figure. They largely deviate from the observed strain curve. Therefore, it can be presumed that the decrease in ϕ or the strain of the specimen after the region of initiating the $\overline{A}_2$ process is brought about by neither the γ_F and γ_C (case 1) nor the γ_F (case 2-1). Thus, the assumption of the molecular process of case 2-2, in which the microfibrils are stretched and therefore the crystallites are newly formed in uniaxial extension, as decribed later in more detail, may be acceptable. The curves of case 2-2 are obtained by eq. (24) and shown by the two dots–dash lines in Figure 12. This model is also supported experimentally by the fact that the long period observed by SAXS depends on the testing temperature after the $A_2 \rightarrow \overline{A}_2$ transition takes place, as shown in Figure 9, and that the curve of the thickness of the crystallites evaluated by eq. (1) deviates from the calculated curve after the $A_2 \rightarrow \overline{A}_2$ transition takes place, as described previously.

In the extension for $\theta = 90°$ at 100°C, as shown in Figure 12(d), the calculated curve on the basis of eq. (18) is lower than the observed one in the vicinity of the region of initiating deformation. Therefore, it is necessary to take into account of another deformation process in this region, in addition to the A_1 and A_2 processes. It must be considered from this point of view that the specimen will be strained by both the A_1 and A_2 processes as well as by the deformation mechanism whereby the crystallites of weak strength are preferentially degraded in this region of deformation.

Figure 13 shows the relationship between the shearing stress acting on the crystallite boundary, τ, and e_W in the same testing conditions as in Figure 12. The shearing stress τ, is given by

$$\tau = (\sigma_0/2) \sin 2\phi \tag{25}$$

where σ_0 is the tensile true stress acting along the testing direction; τ is the most effective shearing stress for causing the intercrystallite boundary slip. Since the τ value takes a maximum approximately near the region of initiating the $\overline{A}_2$

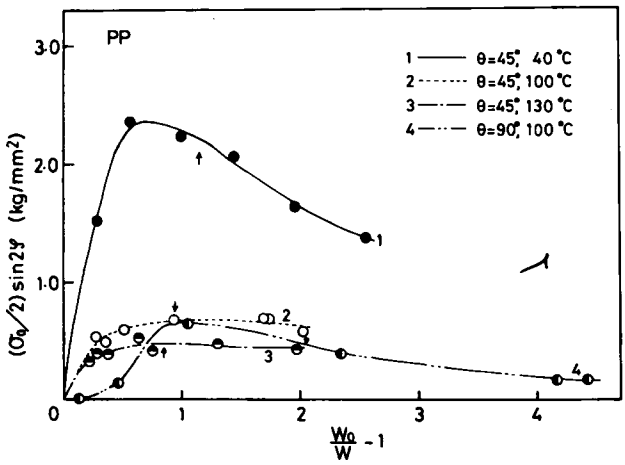

Fig. 13. Relationships between the shearing stress acting on the crystallite boundary, $(\sigma_0/2) \sin 2\phi$, and e_W in uniaxial extension for $\theta = 45°$ at 40°C, 100°C, and 130°C and for $\theta = 90°$ at 100°C. Arrows in the figure show $(\sigma_0/2) \sin 2\phi$ at the regions of initiating $\overline{A}_2$ process.

process and decreases after this region, the amount of the deformation associated with the A_1 process becomes small after this region. This view supports the result in Figure 12.

Change in Normal Stress Acting Along the Molecular Axis During Uniaxial Extension After the $A_2 \rightarrow \overline{A}_2$ Transition

Figure 14 shows the relationship between the normal stress acting along the molecular axis, σ, and the strain of the microfibrils in case 2-2, e_F, after the $A_2 \rightarrow \overline{A}_2$ transition takes place under the same testing conditions as in Figure 12. This tensile stress σ is given by

$$\sigma = \sigma_0(1 + \cos 2\phi)/2 \tag{26}$$

Also, the strain of the microfibrils in case 2-2, e_F, is

$$e_F = (W_i/W_{obs}) - 1 \tag{27}$$

The solid lines in Figure 14 are the σ curves observed, while the dotted lines are the ones calculated by

$$\sigma = \sigma_i(1 + e_F) \tag{28}$$

where σ_i is the normal stress at the region of initiating $\overline{A}_2$ process. It is assumed in eq. (28) that the specimen is deformed only by the molecular process of pulling out of the folded chains in the crystalline region by being stretched by the tie molecules, and the σ value is proportional to the fraction of the tie molecules, that is, the number of tie molecules per total number of chain stems in a crys-

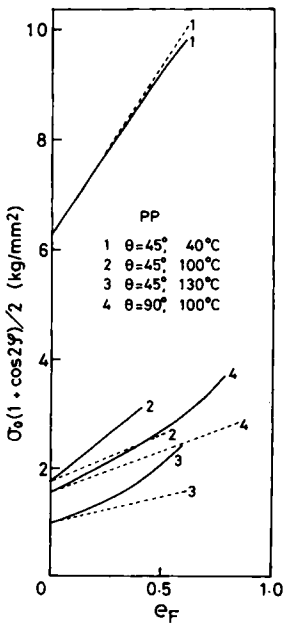

Fig. 14. Relationship between the normal stress acting along the molecular axis, $(\sigma_0/2)(1 + \cos 2\phi)$, and the strain of microfibrils in case 2-2, e_F, after the $A_2 \rightarrow \overline{A}_2$ transition takes place in uniaxial extension for $\theta = 45°$ at 40°C, 100°C, and 130°C and for $\theta = 90°$ at 100°C. Solid lines are the $(\sigma_0/2)(1 + \cos 2\phi)$ curves experimentally determined, and dotted lines are the ones calculated by eq. (28).

tallite. Furthermore, it is assumed that the width reduction is much larger than the thickness reduction and that the volume of the specimen does not remarkably change in uniaxial extension.[9] Then

$$e_F \simeq \{(A_i/A_{obs}) - 1\} \simeq \{(W_i/W_{obs}) - 1\}$$

where A_i and A_{obs} are the cross sections of the specimen at the $A_2 \rightarrow \bar{A}_2$ transition and after the transition, respectively. As shown in Figure 14, the calculated curves shown by dotted lines deviate more and more from the solid lines of the observed data with increasing strain of the microfibrils in uniaxial extension for $\theta = 45°$ at 100°C, for $\theta = 45°$ at 130°C, and for $\theta = 90°$ at 100°C.

This fact can be also interpreted by the tie molecules newly formed during extension on the basis of the following molecular process: After the folded chains are pulled out of the crystallites by overcoming the intermolecular force to restrain them in the crystallites and conformationally change into extended chains, these extended chains refold to bury other extending chain, and then the tie molecules shown by the arrows in Figure 15 are newly formed. The ability for sustaining a load in the tie molecule designated 2 is higher than in the tie molecules designated 1 and 3. Therefore, from Figure 14 it may be assumed that after the initiation of the $\bar{A}_2$ process the fraction of the extending chains is increased and much more of the type 2 tie molecule is formed.

On the other hand, the σ curve calculated is slightly lower than the one observed in uniaxial extension at $\theta = 45°$ at 40°C, as shown in curve 1 in Figure 14. This may be caused by the scission of tie molecules during deformation, which takes place more easily at the testing temperature of 40°C, being below the temperature of crystalline relaxation, which is located about 110°C (138 Hz).[13-15]

Change in γ_F and γ_C During Uniaxial Extension

Figures 16(a) and 16(b) show the relationship of γ_F versus e_W and γ_C versus e_W, respectively, in extension for $\theta = 45°$ at 40 °C, for $\theta = 45°$ at 100°C, for $\theta = 45°$ at 130°C, and for $\theta = 90°$ at 100°C before the $A_2 \rightarrow \bar{A}_2$ transition takes place. Before the $A_2 \rightarrow \bar{A}_2$ transition takes place in extension for $\theta = 45°$, both the A_1 and A_2 processes contribute to the total strain of the specimen, as shown in Figure

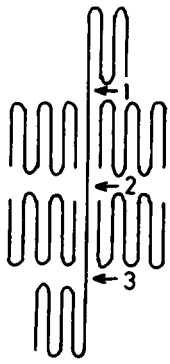

Fig. 15. Schematic representation of tie molecules newly formed in uniaxial extension of crystalline polymers.

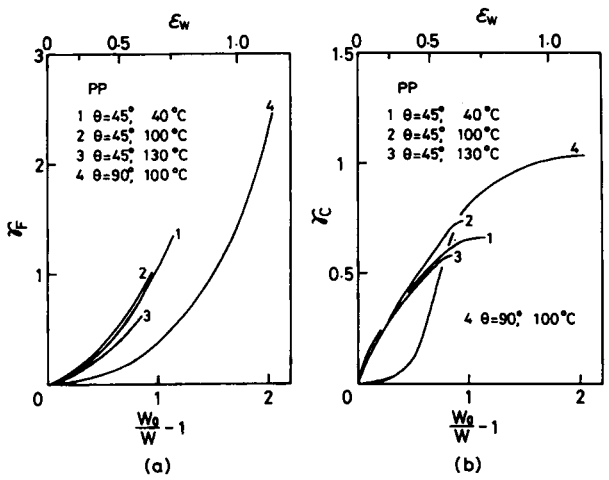

Fig. 16. Relationship (a) between γ_F and e_W and (b) between γ_C and e_W in uniaxial extension for $\theta = 45°$ at 40°C, 100°C, and 130°C and for $\theta = 90°$ at 100°C.

12, and both eqs. (16) and (17) approximately describe the superstructural change of the specimen. It becomes apparent that both γ_F and γ_C in extension of the T-die sheet of isotactic polypropylene for $\theta = 45°$ are almost independent of the testing temperature. Both γ_F and γ_C in extension for $\theta = 90°$ at 100°C are less than for $\theta = 45°$ at the initial region of deformation, but increase with increasing e_W after this region of deformation. This fact confirms that the crystallites whose strength is lower are preferentially destroyed without the deformation due to the A_1 and A_2 processes. The normal stress effectively acts perpendicular to the molecular axis, and the shearing stress acting along the molecular axis is very small in the initial region of deformation.

Initial Shear Compliances for the A_1 and A_2 Processes

Figure 17 shows the relationship between the shearing stress τ acting along the molecular axis on the crystallite boundary given by eq. (25) and γ_F or γ_C calculated by eqs. (16) or (17) in the same testing conditions as in Figure 12. The initial shear compliance for the A_1 process is lower than for the A_2 process in each testing condition. Both the initial shear compliances for the γ_F and γ_C increase if the testing temperature becomes high. At a testing temperature of 100°C, the initial shear compliances for the γ_F and γ_C for $\theta = 90°$ are higher than the ones for $\theta = 45°$, since the normal stress acting perpendicular to the molecular axis for $\theta = 90°$ is larger. Both the distance between the molecular chains in crystallites and the one between the crystallite boundaries increase, and thus both the A_1 and A_2 processes take place more easily.

The shearing stress τ increases little or decreases with increasing γ_F or γ_C in the vicinity of the $A_2 \rightarrow \bar{A}_2$ transition. This is the so-called yield phenomenon, where folded chains may be pulled out of crystallites by tension of tie molecules.

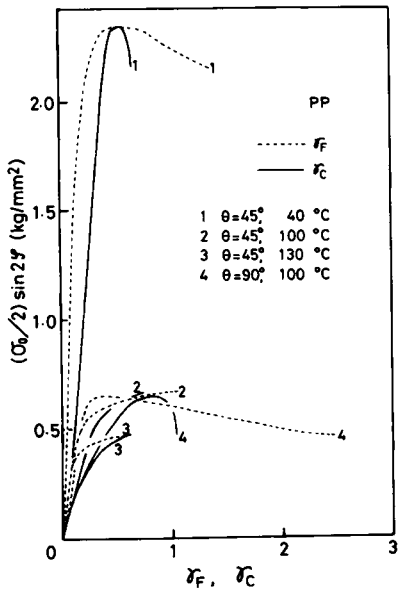

Fig. 17. Relationship between the shearing stress acting along the molecular axis on the crystallite boundary, $(\sigma_0/2)\sin 2\phi$, given by eq. (25) and γ_F or γ_C calculated by eq. (16) or (17) in uniaxial extension for $\theta = 45°$ at 40°C, 100°C, and 130°C and for $\theta = 90°$ at 100°C.

CONCLUSION

The superstructural change in the uniaxial extension of the T-die sheet of isotactic polypropylene can be analyzed by WAXD and SAXS. Both the A_1 process (intercrystallite boundary slip) and the A_2 process (uniform shear deformation of crystallites) take place in an earlier stage of extension, and the $\overline{A}_2$ process (restoration of molecular orientation from the shear-deformed state) does so in a latter stage of extension. Furthermore, the strains of the preoriented isotactic polypropylene associated with the A_1, A_2, and $\overline{A}_2$ processes are quantitatively evaluated as a function of total strain. The superstructural change of the preoriented isotactic polypropylene in uniaxial extension for $\theta = 45°$ at 40°C, for $\theta = 45°$ at 100°C, for $\theta = 45°$ at 130°C, and for $\theta = 90°$ at 100°C is analyzed on the basis of the changes in strains of the A_1, A_2, and $\overline{A}_2$ processes as a function of macroscopic strain of the specimen. It can be concluded that:

1. Both the A_1 and A_2 processes predominantly take place in uniaxial extension for $\theta = 45°$ before the $A_2 \rightarrow \overline{A}_2$ transition takes place. But in addition of the A_1 and A_2 processes, the crystallites of lower strength are preferentially degraded in extension for $\theta = 90°$ before the $A_2 \rightarrow \overline{A}_2$ transition takes place.

2. After the $A_2 \rightarrow \overline{A}_2$ transition takes place, the microfibrils are preferentially deformed by the molecular process such as pulling out folded chains of crystallites to provide the extending chains, being followed by their refolding. This deformation process is supported by the fact that the thickness of crystallites depends on the testing temperature after the $A_2 \rightarrow \overline{A}_2$ transition takes place.

3. The normal stress acting parallel to the molecular axis is rapidly increased by newly formed tie molecules after the $A_2 \rightarrow \overline{A}_2$ transition takes place.

4. The initial shear compliance for the A_1 process is always smaller than for the A_2 process under all the testing conditions.

References

1. A. Peterlin, *J. Mater. Sci.*, **6**, 490 (1971).
2. A. Keller and D. P. Pope, *J. Mater. Sci.* **6**, 453 (1971).
3. D. P. Pope and A. Keller, *J. Polym. Sci. A-2*, **13**, 533 (1975).
4. S. Maruyama, K. Imada, and M. Takayanagi, *Int. J. Polym. Mater.*, **1**, 211 (1972).
5. T. Nagamura, K. Fukitani, and M. Takayanagi, *J. Polym. Sci. A-2*, **13**, 1515 (1975).
6. K. Yamada and M. Takayanagi, *Kobunshi Ronbunshu*, **32**, 724 (1975).
7. A. Peterlin, *Pure Appl. Chem.*, **39**, 239 (1974).
8. K. Yamada and M. Takayanagi, *Kobunshi Ronbunshu*, **34**, 53 (1977).
9. K. Yamada and M. Takayanagi, *Kobunshi Ronbunshu*, **34**, 465 (1977).
10. F. Danusso, G. Moraglio, and G. Natta, *Ind. Plast. Mod.*, **10**, 40 (1958).
11. R. J. Young, P. B. Bowder, J. M. Ritchie, and J. G. Rider, *J. Mater. Sci.*, **8**, 23 (1973).
12. M. Takayanagi and K. Yamada, in *Proceedings of the 7th International Congress on Rheology*, C. Klason and J. Kubát, Eds., Gothenburg, 1976, p. 252.
13. J. Becht, *J. Polym. Sci. C*, **32**, 319 (1971).
14. H. H. Kausch and D. Langbein, *J. Polym. Sci. A-2*, **11**, 1201 (1973).
15. S. Minami, J. Tanoue, and M. Takayanagi, *Kogyo-Kagaku-Zasshi*, **69**, 90 (1965).

Received October 12, 1978